Journal of Physical Science Vol. 36(2), 1–18, 2025



Determination of the Transport Coefficients of an Air Plasma Contaminated by AgSnO₂ Alloy Vapour

Adjigkiga Banouga,¹* Wêpari Charles Yaguibou,¹ Abdoul Karim Kagoné,¹ Ibrahim Pafadnam,¹ Niéssan Kohio,² Zacharie Koalaga¹ and François Zougmoré¹

¹Université Joseph Ki-Zerbo, Physique, LAME, Ouagadougou, Burkina Faso ²Université Joseph Ki-Zerbo, Physique, LAME, Institut des Sciences, Ouagadougou, Burkina Faso

*Corresponding author: adjigkiga.banouga@ujkz.bf

Published online: 29 August 2025

To cite this article: Banouga, A. et al. (2025). Determination of the transport coefficients of an air plasma contaminated by AgSnO₂ alloy vapour. *J. Phys. Sci.*, 36(2), 1–18. https://doi.org/10.21315/jps2025.36.2.1

To link this article: https://doi.org/10.21315/jps2025.36.2.1

ABSTRACT: The physicochemical properties of the electric arc determine the success or failure of the electric current by the circuit breaker. This work is devoted to the determination of the transport coefficients of air plasma contaminated by silver tin(IV) oxide (AgSnO₂) alloy electrical contact vapour in a low voltage circuit breaker. It aims to theoretically evaluate the influence of AgSnO₂ alloy electrical contact material on the electrical current breaking capacity of the low-voltage air circuit breaker through the electrical conductivity, thermal conductivity and dynamic viscosity of the plasma air-AgSnO₂. They are determined over a temperature range from 500 K -30,000 K, at atmospheric pressure and at local thermodynamic equilibrium. The analytical expressions necessary to determine these transport coefficients of the air-AgSnO₂ mixture plasma are deduced from the Boltzmann equation using the approximate Chapman-Enskog method. Analyses of the obtained results show that, for the same given temperature, the electrical conductivity increases significantly when the AgSnO₂ alloy vapour increases in the mixture for temperatures below 11,000 K. The dynamic viscosity of the plasma decreases as the percentage of AgSnO₂ alloy electrical contact vapour increases in the mixture, for temperatures below 12,000 K. In the temperature range from 500 K-20,000 K, the total thermal conductivity of the plasma decreases as the percentage of AgSnO₂ alloy electrical contact vapour increases in the mixture. It results that increasing the percentage of electrical contact vapour in AgSnO2 alloy will slow down the extinction of the electric arc created inside the circuit breaker, especially beyond 0.1% of vapour. This slowing down of the extinction of the electric arc can cause the circuit breaker to fail to cut off electrical current.

Keywords: circuit breaker, plasma, electric arc, transport coefficients, AgSnO₂ electrical contact

1. INTRODUCTION

The success or failure of the circuit breaker cutting the electrical current depends heavily on the physicochemical properties of the electric arc created inside the circuit breaker. Improving the performance and optimising the efficiency of the air circuit breaker requires a good knowledge of the physico-chemical phenomena involved when the electrical current is cutting. Which are influenced by the vapours from the electrodes (electrical contacts).

Studies carried on electrical contacts such as copper (Cu), silver (Ag), silver–tungsten carbide (AgWC), have shown that the behaviour of the electric arc changes depending on the nature of the circuit breaker electrodes. ¹⁻⁶

Several studies have been carried on tin dioxide (SnO₂) sensors doped with noble metals such as palladium (Pd) and nickel (Ni) for the detection of a wide variety of toxic, combustible and industrial gases.⁷⁻⁹

We chose to focus on the alloy of silver and tin dioxide (AgSnO₂) because it is used more and more these days for electrical inspections of the low voltage circuit breakers. In addition, it has strong resistance to electric arc erosion and has good anti-electric welding properties. ^{10–13}

In this work, we are interested in the transport coefficients of air-AgSnO₂ plasma such as electrical conductivity, thermal conductivity and dynamic plasma viscosity. Knowledge of these transport coefficients is very important for electric arc plasma modeling. ¹⁴ They also can be used to evaluate the arc extinguishing performance. The effectiveness of the electrical current cut-off by the circuit breaker strongly depends on the thermal and electrical characteristics of the extinguishing medium. It is therefore appropriate to choose as extinguishing medium, a medium simultaneously presenting at least the following characteristics with regard to its transport coefficients: ¹⁵

- low electrical conductivity that decreases with temperature;
- high thermal conductivity.

The paper calculates the transport coefficients of air- $AgSnO_2$ thermal plasma mixtures existing in the low voltage circuit breaker devices, in order to better understand the behaviour of the electric arc during its lifetime. The medium is pure air, with the $AgSnO_2$ metal vapours coming from the electrodes.

2. ANALYTICAL EXPRESSIONS

The necessary analytical expressions that we use to determine the transport coefficients of the air-AgSnO $_2$ mixture plasma, are deduced from the Boltzmann equation using the approximate Chapman-Enskog method. The plasma transport coefficients are linked to collision integrals relating to the various interactions between the particles present in the mixture.

The equilibrium composition of the plasmas studied necessary for the calculation of the different quantities is given by Banouga et al.¹⁶ In the plasma of mixtures of air, silver and tin dioxide studied, we took into account 40 chemical particles:

The electron and the monatomic particles are in total 17:

```
    electron (e<sup>-</sup>), Ag<sup>-</sup>, nitrogen (N<sup>-</sup>), oxygen (O<sup>-</sup>), tin (Sn<sup>-</sup>), Ag, N, O, Sn, Ag<sup>+</sup>,
    N<sup>+</sup>, O<sup>+</sup>, Sn<sup>+</sup>, Ag<sub>2</sub><sup>+</sup>, N<sub>2</sub><sup>+</sup>, O<sub>2</sub><sup>+</sup>, Sn<sub>2</sub><sup>+</sup>;
```

The diatomic particles are a total of 11:

```
– N_2^-, O_2^-, nitric oxide (NO<sup>-</sup>), NO, N_2, O_2, tin(II) oxide (SnO), Sn_2, NO<sup>+</sup>, N_2^+, O_2^+;
```

The triatomic particles and more are in total 12:

```
nitrate(NO_3^-), nitrite (NO_2^-), dinitrogen pentoxide (N_2O_5), dinitrogen tetroxide (N_2O_4), dinitrogen trioxide (N_2O_3), nitrogen trioxide (NO_3), nitrogen dioxide (NO_2), dinitrogen oxide (N_2O_3), N_3, N_3, N_3, N_3, N_3, N_3, N_3.
```

In their work, Colombo et al. showed that the simplified expressions of Devoto can be used well for the calculation of plasma transport coefficients. 17–20

2.1 Transport Coefficients

2.1.1 Electrical conductivity coefficient

The electrical conductivity of a plasma measures its ability to conduct electric current. The mobility of ions being low compared to that of electrons, the electrical conductivity of the plasma is essentially ensured by the electrons. It can be expressed from the order 3 approximation of the Chapman-Enskog method by the following relation: 14,21–23

$$\sigma = \frac{3}{2} e^{2} n_{e}^{2} \left(\frac{2\pi}{kT m_{e}}\right)^{\frac{1}{2}} \frac{\begin{vmatrix} q^{11} & q^{12} \\ q^{12} & q^{22} \end{vmatrix}}{\begin{vmatrix} q^{00} & q^{01} & q^{02} \\ q^{10} & q^{11} & q^{12} \\ q^{20} & q^{21} & q^{22} \end{vmatrix}}$$

$$(1)$$

where k is the Boltzmann constant, e the elementary charge (C), m_e the mass (kg) of the electron and n_e the number density (m^3) of the electrons. The terms q^{ij} are expressed in function of number densities of particles and average particles collision cross sections.

2.1.2 Thermal conductivity coefficient

Thermal conductivity represents the ability of materials or gas mixtures to conduct heat. The total thermal conductivity can be written as the sum of:

- the thermal conductivity of translation, due to the translation of heavy particles λ_{tr}^{h} and electrons λ_{tr}^{e} :
- the thermal conductivity of reaction $\lambda_{\rm reac}$, due to the various chemical reactions;
- the internal thermal conductivity, due to internal molecular energies.

So, we have:

$$\lambda_{\text{tot}} = \lambda_{\text{tr}}^{\text{h}} + \lambda_{\text{tr}}^{\text{e}} + \lambda_{\text{reac}} + \lambda_{\text{int}}$$
 (2)

The translational thermal conductivity of heavy particles is obtained for an approximation of order 2 of the Chapman-Enskog method by the following expression:^{21,24–27}

$$\lambda_{tr}^{h} = 4 \frac{\begin{vmatrix} L_{11} & \dots & L_{1N} & X_{1} \\ \dots & L_{ii} & \dots & \dots \\ L_{N1} & \dots & L_{NN} & X_{N} \\ X_{1} & \dots & X_{N} & 0 \end{vmatrix}}{\begin{vmatrix} L_{11} & \dots & L_{1N} \\ \dots & L_{ii} & \dots \\ L_{N1} & \dots & L_{NN} \end{vmatrix}}$$
(3)

where N is the total number of particles and the mole fraction (X_i) of particle i. The L_{ij} terms are expressed as a function of the molar masses (M_i) (kgmol⁻¹) and the collision integrals $(\overline{\Omega}_{ij}^{(l,s)})(m^2)$.

The thermal conductivity of electron translation is obtained in an approximation of order 3 by the Chapman-Enskog method by the following expression: 17,24

$$\lambda_{\rm tr}^{\rm e} = \frac{75}{8} n_{\rm e}^2 k \left(\frac{2\pi kT}{m_{\rm e}} \right)^{\frac{1}{2}} \frac{q^{22}}{q^{11} q^{22} - (q^{12})^2}$$
 (4)

where n_e and m_e are respectively the number density (m⁻³) and the mass (kg) of the electrons. The terms, q^{11} , q^{12} and q^{22} and are expressed in terms of the number densities and the average collision cross sections of the particles.

The reaction thermal conductivity can be expressed to the first order of the Chapman-Enskog method by the following relation:^{21,28–30}

$$\lambda_{\text{reac}} = \frac{-1}{RT^2} \frac{\begin{vmatrix} A_{11} & \dots & A_{1\mu} & \Delta H_1 \\ \dots & \dots & \dots \\ A_{\mu 1} & \dots & A_{\mu \mu} & \Delta H_{\mu} \\ \Delta H_1 & \dots & \Delta H_{\mu} & 0 \end{vmatrix}}{\begin{vmatrix} A_{11} & \dots & A_{1\mu} \\ \dots & \dots & \dots \\ A_{\mu 1} & \dots & A_{\mu \mu} \end{vmatrix}}$$

$$A_{11} & \dots & A_{\mu \mu}$$
(5)

where R is the ideal gas constant, ΔH_i represents the enthalpy change (Jmol⁻¹) due to the chemical reaction and μ the number of chemical reactions.

The internal thermal conductivity can be expressed by the following relationship: 17,31-34

$$\lambda_{\text{int}} = \sum_{i=1}^{\mu} \frac{\left[(\lambda_{\text{int}})_{i} \right]}{\left[1 + \sum_{\substack{j=1 \ j \neq i}}^{\mu} \frac{D_{ii}}{D_{ij}} \frac{X_{j}}{X_{i}} \right]}$$
(6)

where $(\lambda_{int})_i$ is the internal thermal conductivity of the chemical particle i.

From the study of several gases, Hertz proposes an empirical relationship linking the electric arc time constant τ to the maximum coefficient of thermal conductivity of reaction λ_{reac} of the gas given by the following expression:^{14,35}

$$\tau \lambda_{\text{reac}}^{\text{max}} = C^{\text{te}}$$
 (7)

This relationship shows that the more the maximum of λ_{reac} increases, the more the life of the electric arc decreases.

2.1.3 Dynamic viscosity coefficient

The dynamic viscosity of a plasma characterises its resistance to flow. It strongly depends on heavy particles. Dynamic viscosity can be expressed by the following relationship:^{21,31,36,37}

$$\eta = -\frac{\begin{vmatrix} H_{11} & \dots & H_{1\mu} & X_1 \\ \dots & \dots & \dots & \dots \\ H_{\mu 1} & \dots & H_{\mu \mu} & X_{\mu} \\ X_1 & \dots & X_{\mu} & 0 \end{vmatrix}}{\begin{vmatrix} H_{11} & \dots & H_{1\mu} \\ \dots & \dots & \dots \\ H_{\mu 1} & \dots & H_{\mu \mu} \end{vmatrix}}$$
(8)

The matrix elements H_{ii} and H_{ij} are expressed as a function of M_i , collision integrals $\overline{\Omega}_{ij}^{(1,s)}(m^2)$ and X_i .

2.2 Collision Integrals

2.2.1 Neutral - ion and electron - neutral particles interactions

To determine the values of the collision integrals of ion - neutral particles interactions, such as: $Ag - O^+$; $Ag - Sn^+$; $NO^+ - O$; $Ag - Sn^+$; $NO_2 - N^-$; $O - Sn_2^+$; $Ag - N^-$; $N_2 - Ag_2^+$; $O_2 - Sn^+$; $N_2O - N^+$, we use the collision integrals given by: 15,36,38,39

$$\overline{\Omega}_{ij}^{(l,s)} = \frac{4(1+s)}{(s+1)![2l+1-(-1)']} \left(\frac{\alpha_i Z_j^2 e^2}{2\pi \varepsilon_0 kT}\right)^{\frac{1}{2}} \Gamma\left(s+\frac{3}{2}\right) A_{(4)}^{(1)}$$
(9)

with, $A_{(4)}^{(1)} = 0,6547$, $A_{(4)}^{(2)} = 0,3852$, $A_{(4)}^{(3)} = 0,7166$. Z_i is the charge number of the charged particle j, e the elementary charge (C), α_i the polarisability of the neutral particle i and ε_0 the permittivity of the vacuum.

We also use fitting polynomials from the work of André et al. to determine the collision integrals of electron - neutral and neutral - neutral particles, for example:^{32,40}

$$e^{-} - O; e^{-} - N; e^{-} - N_{2}; e^{-} - N_{2}O; e^{-} - NO; e^{-} - O_{2}; e^{-} - Ag.$$

$$\overline{Q}_{ij}^{(l,s)} = \alpha_{1} \ln(T) + \alpha_{2} + \alpha_{3}T + \alpha_{4}T^{-1} + \alpha_{5}T^{-2} + \alpha_{6}T^{-3} + \alpha_{7}T^{-4}$$
(10)

The coefficients α_i for different particles are taken from the same reference.

2.2.2 Neutral - neutral particles interactions

We use the collision integrals given by Neufeld's empirical formula to determine the values of the collision integrals of neutral - neutral particle interactions, such as:⁴¹⁻⁴³

$$\begin{split} &N-N NO-N_2O; O_2-N_2; N_2O-N_2; Ag-Ag; O-O; NO-N_2; O-N; \\ &N_2-N_2; NO_2-O; O_2-O_2; NO-NO; N_2O-N_2O; Ag-N; Ag-O; Ag-NO; Ag-N_2; Ag-NO; Ag-N_2; Ag-NO; Ag-N_2; Ag-NO; Ag-N_2; Ag-NO; Ag-N_2; Ag-NO; Ag-N_2; Ag-NO; Ag-N_2O. \end{split}$$

$$\overline{\Omega}_{ij}^{(l,s)} = r_0^2 \left[\frac{A}{T^{*B}} + \frac{C}{\exp(DT^*)} + \frac{E}{\exp(FT^*)} + \frac{G}{\exp(HT^*)} + RT^{*B}\sin(ST^{*W} - P) \right] (11)$$

 r_o is the distance (m) for which the potential is zero and T^* the temperature reduced which varies from 0–200. ^{14,44} The values from A to W are tabulated as a function of (1,s). ⁴¹

2.2.3 Charged - charged particles interactions

To determine the values of the collision integrals of charged - charged particles interactions, such as:

$$\begin{array}{l} Ag^{\scriptscriptstyle +} - Ag_{\scriptscriptstyle 2}{^{\scriptscriptstyle +}} \, ; \, Ag_{\scriptscriptstyle 2}{^{\scriptscriptstyle +}} - Ag_{\scriptscriptstyle 2}{^{\scriptscriptstyle +}} \, ; \, O^{\scriptscriptstyle -} - N^{\scriptscriptstyle +} \, ; \, NO^{\scriptscriptstyle +} - O_{\scriptscriptstyle 2}{^{\scriptscriptstyle +}} \, ; \, Sn^{\scriptscriptstyle +} - O^{\scriptscriptstyle +} \, ; \, N_{\scriptscriptstyle 2}{^{\scriptscriptstyle +}} - N^{\scriptscriptstyle -} \, ; \, O_{\scriptscriptstyle 2}{^{\scriptscriptstyle +}} - Ag^{\scriptscriptstyle +} \, ; \\ O_{\scriptscriptstyle 2}{^{\scriptscriptstyle +}} - Ag_{\scriptscriptstyle 2}{^{\scriptscriptstyle +}} \, ; \, Sn_{\scriptscriptstyle 2}{^{\scriptscriptstyle +}} - N^{\scriptscriptstyle -} \, ; \, O^{\scriptscriptstyle -} - N^{\scriptscriptstyle -} \, ; \, O_{\scriptscriptstyle 2}{^{\scriptscriptstyle +}} - Sn_{\scriptscriptstyle 2}{^{\scriptscriptstyle +}} \, ; \, e^{\scriptscriptstyle -} - e^{\scriptscriptstyle -} \, ; \, N^{\scriptscriptstyle +} - N_{\scriptscriptstyle 2}{^{\scriptscriptstyle +}} \, ; \, Sn^{\scriptscriptstyle +} - N^{\scriptscriptstyle +} , \, \text{we} \\ \text{use the collision integrals given by:} \end{array}$$

$$\begin{cases}
\overline{\Omega}_{ij}^{(l,s)} = \left[\frac{4}{s(s+1)}\right] b_0^2 \left[\ln\left(\frac{2\lambda_D}{b_0}\right) - \frac{1}{2} - 2\overline{\gamma} + \psi(s)\right] \\
\overline{\Omega}_{ij}^{(2,s)} = \left[\frac{12}{s(s+1)}\right] b_0^2 \left[\ln\left(\frac{2\lambda_D}{b_0}\right) - 1 - 2\overline{\gamma} + \psi(s)\right] \\
\overline{\Omega}_{ij}^{(3,s)} = \left[\frac{12}{s(s+1)}\right] b_0^2 \left[\ln\left(\frac{2\lambda_D}{b_0}\right) - \frac{7}{6} - 2\overline{\gamma} + \psi(s)\right] \\
\overline{\Omega}_{ij}^{(4,s)} = \left[\frac{16}{s(s+1)}\right] b_0^2 \left[\ln\left(\frac{2\lambda_D}{b_0}\right) - \frac{4}{3} - 2\overline{\gamma} + \psi(s)\right]
\end{cases}$$
with,
$$\begin{cases}
b_0 = \frac{|Z_i Z_j| e^2}{2kT} \\
\psi(s) = \sum_{n=1}^{s-1} \frac{1}{n} ; \lambda_D = \left(\frac{\mathcal{E}_0 k}{e^2} \sum_{i=1}^{N} \frac{T}{Z_i^2 n_i}\right)^{\frac{1}{2}} \\
\psi(1) = 0
\end{cases}$$

$$\psi(1) = 0 \qquad (13)$$

where γ is the Euler constant, e the elementary charge (C), n_1 the number density (m⁻³) of the particle i and λ_D the Debye length (m). Z_i and Z_i are the charges number of the charged particles i and j. In collision integrals $\overline{\Omega}_{ij}^{(1,s)}$, the parameter 1 is greater than or equal to s (s \leq 1), 1 takes the values 1 = 1, 2, 3, 4.

3. RESULTS AND DISCUSSIONS

In this part, we present the results of the plasma transport coefficients of mixtures of air, Ag and SnO₂ for different percentages of the mixture. They are determined at local thermodynamic equilibrium (LTE) in a temperature range from 500 K–30,000 K and at atmospheric pressure. The AgSnO₂ alloy electrical contact material, used in this study, is composed of 4% SnO₂ and 96% Ag. In fact, metal oxides of the SnO₂ type (3.3%–14% maximum) aim to reduce the risks of welding in the cutting device, but their addition in large quantities greatly increases the duration of the electric arc thus aggravating the erosion of the electrical contacts. ^{6,10,46} We considered mass percentages. We have studied the thermodynamic properties

of these plasmas in our article Banouga et al. 46 The mass density varies from 0.0024 kgm $^{-3}$ –1.0406 kgm $^{-3}$, at atmospheric pressure, depending on the percentage of AgSnO₂ and the temperature of the mixture.

In order to validate our calculation code, we calculated and compared our results of transport coefficients, from air plasma to atmospheric pressure and LTE with those of Capitelli et al. and Boulos et al., in Figures 1–3.^{47,48}

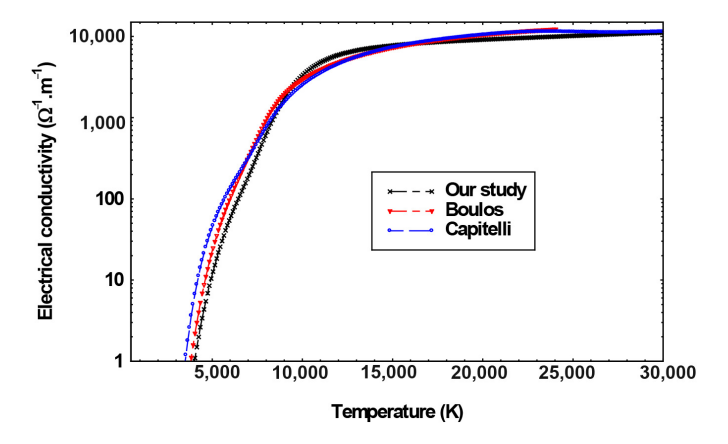


Figure 1: Comparison of the results of the electrical conductivity of air plasma at atmospheric pressure and the LTE of Capitelli, Boulos and our study.

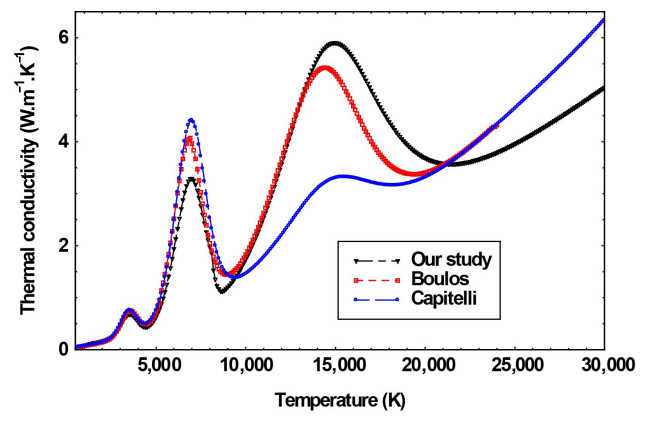


Figure 2: Comparison of the results of the thermal conductivity of air plasma at atmospheric pressure and the LTE of Capitelli, Boulos and our study.

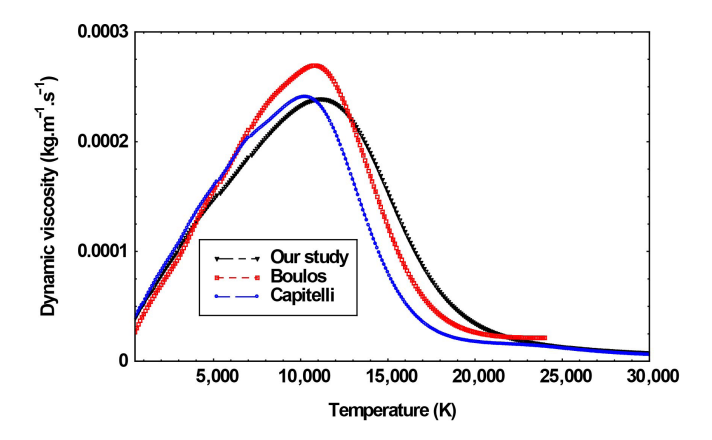


Figure 3: Comparison of the results of the dynamic viscosity of air plasma at atmospheric pressure and the LTE of Capitelli, Boulos and our study.

In Figure 1 which presents the electrical conductivity, we see differences which vary from 0%–15% between our results and those of Capitelli, and from 0%–9% between our results and those of Boulos, for temperatures lower than 10,000 K. The differences vary from 0%–5% between our results and those of Boulos for temperatures between 10,000 K–24,000 K, and between our results and those of Capitelli for temperatures between 10,000 K–30,000 K.

In Figure 2 which presents the thermal conductivity, for temperatures below $8,000~\rm K$, we observe that the differences between our results and those of Capitelli and Boulos vary from 0%-10%. For temperatures between $8,000~\rm K-24,000~\rm K$ the differences vary from 0%-15% between our results and those of Boulos, and for temperatures between $8,000~\rm K-30,000~\rm K$ the differences vary from 0%-20% between our results and those of Capitelli.

In Figure 3 which presents the dynamic viscosity, we see that differences between our results and those of Capitelli and Boulos for temperatures below 9,000 K vary from 0%–8%. For temperatures between 9,000 K–24,000 K, the differences between our results and those of Boulos vary from 0%–10%, but the differences between our results and those of Capitelli vary from 0%–15% for temperatures between 9,000 K–30,000 K.

The observed differences can be explained, among other things, by the following reasons:

• the input data required for the calculations of the interaction potentials such as the Lennard-Jones potential, the Coulomb potential of the different particles;

• the input data required to calculate the Debye length and collision integrals of the different particles.

We can say that depending on the temperature zone considered, our results are in fairly good agreement either with those of Capitelli et al. or with those of Boulos et al. 47,48

Figure 4 presents the evolution of the electrical conductivity of plasmas of air-AgSnO $_2$ mixtures, as a function of temperature, atmospheric pressure and the LTE, for different percentages of the mixture.

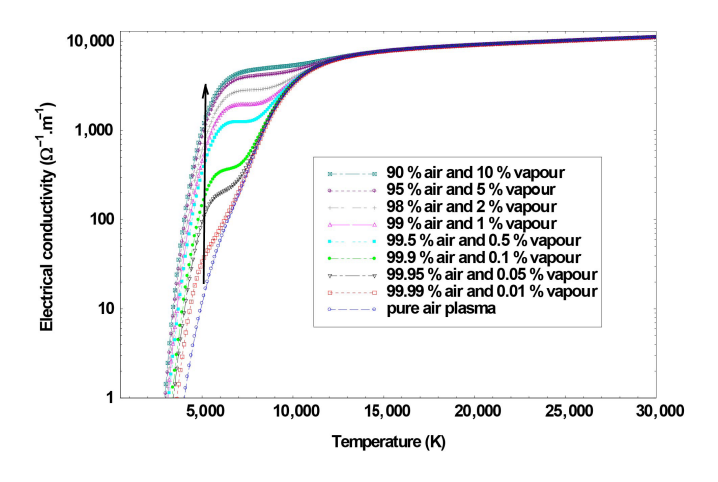


Figure 4: Influence of the percentage of AgSnO₂ alloy vapour on electrical conductivity.

We observe, in Figure 4, that the electrical conductivity of the air plasma is lower than the electrical conductivities of all the other plasmas studied. This phenomenon is very remarkable for temperatures below 10,000 K. For example, at 4,500 K, the air plasma has an electrical conductivity of 4.5485 $\Omega^{-1}m^{-1}$ and for the plasma of the mixture 99.5% air and 0.5% vapour, its value is 11.2572 $\Omega^{-1}m^{-1}$, an increase of 147%. The electrical conductivity being proportional to the square of the number density of the electrons, its increase can be explained by the increase in the number density of the electrons in the mixture. Indeed, when the AgSnO₂ alloy vapour increases in the mixture, the quantity of the chemical elements Sn and Ag also increases. And as the chemical elements Sn and Ag have low first ionisation energy values of 7.34 eV and 7.58 eV, respectively, compared to the chemical elements of air, O and N which respectively have energy values of first ionisation of 13.62 eV and 14.54 eV, the Sn and Ag particles ionise at lower temperatures (below 8,000 K). This causes an increase in the number density of the electrons in the mixture as shown in Figure 4 of Banouga et al. 16

For temperatures between 11,000 K-30,000 K, the various plasmas of air-AgSnO₂ mixtures have almost identical electrical conductivities. This can be explained by the fact that at these high temperatures, the plasmas are almost completely ionised and have almost the same electron density. And as the electrical conductivity is proportional to the numerical density of the electrons, the electrical conductivity undergoes the same behaviour and varies slightly depending on the nature of the plasma considered, for higher temperatures (above 11,000 K).

We note that the increase in the electrical contact vapour of $AgSnO_2$ alloy in the mixture generates a greater increase in electrical conductivity, for temperatures below 11,000 K. Thus, we can note that the electrical contact vapour of $AgSnO_2$ alloy in the mixture, may therefore not be favourable to the cutting of the electric current by the circuit breaker because, depending on its proportion, it contributes to significantly increase the electrical conductivity of the electric arc created, especially at low temperatures (below 11,000 K).

Figure 5 gives the evolution of the total thermal conductivity and its four components, as a function of temperature, atmospheric pressure and the LTE, of the plasma of the mixture of 99.9% air and 0.1% vapour AgSnO₂ alloy.

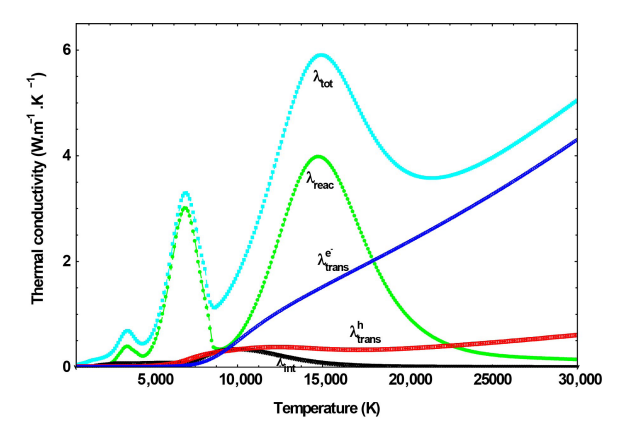


Figure 5: Evolution of the total thermal conductivity and its four components of the plasma of 99.9% air and 0.1% AgSnO₂, as a function of temperature, atmospheric pressure and the LTE.

Figure 5 shows the contribution of each component to the total thermal conductivity. For example at 6,000 K, the translational thermal conductivity of heavy particles, the translational thermal conductivity of electrons, the reaction thermal conductivity and the internal thermal conductivity are 0.1546 W.m⁻¹.K⁻¹, 0.0067 W.m⁻¹.K⁻¹, 1.6888 W.m⁻¹.K⁻¹ and 0.0851 W.m⁻¹.K⁻¹, respectively, for the plasma of the mixture 99.9% air and 0.1% vapour. Which gives a total thermal conductivity 1.9352 W.m⁻¹.K⁻¹.

Figure 6 presents the evolution of the total thermal conductivity of plasmas of air-AgSnO₂ mixtures, as a function of temperature, atmospheric pressure and the LTE, for different percentages of the mixture.

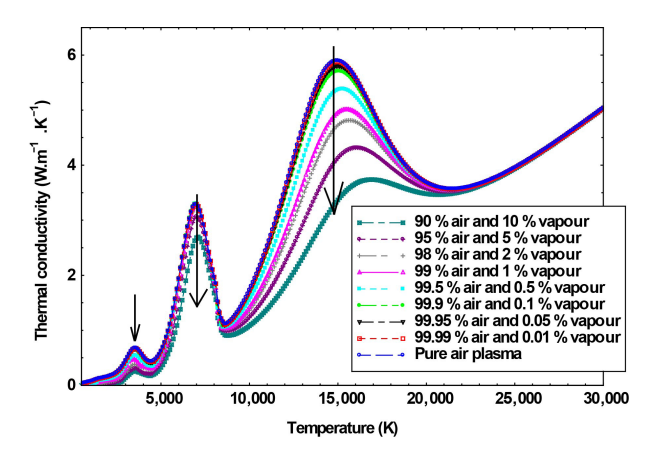


Figure 6: Influence of the percentage of AgSnO₂ alloy vapour on the total thermal conductivity.

In Figure 6, we observe that the total thermal conductivities of the different plasmas have the same looks with the appearance of a first peak around 3,500 K, a second peak around 7,000 K and third peak around 15,000 K. The different chemical reactions which occur in the mixture are responsible for variations in total thermal conductivity.

The peak at 3,500 K corresponds to the dissociations of O_2 and NO molecules and the peak at 7,000 K corresponds to the dissociations of N_2 molecules for the case of air plasma. It corresponds to the dissociations of N_2 molecules and ionisations of Sn, Ag particles (to give Sn⁺, Ag⁺) for the case of air-AgSnO₂ plasmas. The peak appearing at 15,000 K corresponds to the different ionisations of the O, N particles for the case of air plasma. It corresponds to the different ionisations of the particles O, N, Sn⁺, Ag⁺ (to give O⁺, N⁺, Sn₂⁺, Ag₂⁺) for the case of air-AgSnO₂ plasmas.

We see that the total thermal conductivity decreases as the percentage of $AgSnO_2$ alloy vapour increases in the mixture. For example, at 15,000 K the air plasma has 5.8996 W.m⁻¹.K⁻¹ and the plasma of the 90% air and 10% vapour has a total thermal conductivity of 3.3684 W.m⁻¹.K⁻¹, a decrease of 42%.

We can therefore note that the $AgSnO_2$ alloy vapour, depending on its proportion in the mixture, may not be favourable to the cutting of the electric current by the circuit breaker because it contributes to reducing the thermal conductivity of the electric arc created.

Figure 7 presents the evolution of the dynamic viscosity of plasmas of air-AgSnO₂ mixtures, as a function of temperature, atmospheric pressure and the LTE, for different percentages.

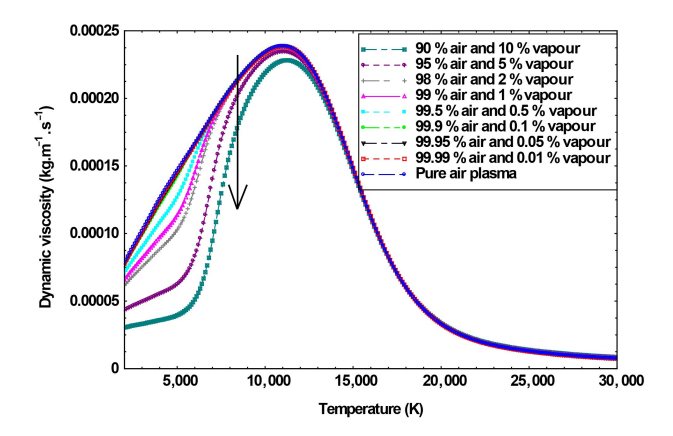


Figure 7: Influence of the percentage of AgSnO₂ alloy vapour on dynamic viscosity.

In Figure 7, we can see that the dynamic viscosity increases at temperatures below 11,000 K, where it reaches its maximum. This peak marks the limit between plasmas more populated with heavy particles (atoms, molecules) and those more populated with light particles (atomic cations). We observe that the dynamic viscosity of the pure air plasma is slightly higher than that of plasmas of mixtures of air and $AgSnO_2$. For example, at 8,500 K, the air plasma has $2.1453 \times 10^{-4} \text{ kgm}^{-1}\text{s}^{-1}$ and the 90% air and 10% steam mixture plasma has a dynamic viscosity value of $1.8188 \times 10^{-4} \text{ kgm}^{-1}\text{s}^{-1}$, a reduction of 15%. This decrease in dynamic viscosity can be explained by the presence of the largest proportion of nitrogen which has a higher ionisation potential than the other particles of the mixture considered.

In the range from 12,000 K to 30,000 K, as the temperature increases, the dynamic viscosity decreases, for the plasmas of the different mixtures. Indeed, when the temperature increases, molecules and atoms gradually disappear through dissociation and ionisation reactions. This therefore results in a decrease in the total number of heavy particles and an increase in the total number of light particles (electrons and atomic cations). This rapid decrease in dynamic viscosity, for the plasmas of different mixtures, can be explained by the progressive disappearance of molecules, then atoms, in the medium.

We note that increasing the AgSnO₂ alloy electrical contact vapour in the mixture contributes to decreasing the dynamic viscosity of the plasma.

4. CONCLUSION

The plasma transport coefficients of the mixture of air and vapour of silver alloy and tin dioxide (AgSnO₂) are determined in a temperature range from 500 K to 30,000 K, at atmospheric pressure and at local thermodynamic equilibrium.

The results obtained show that the increase in the electrical contact vapour of $AgSnO_2$ alloy in the mixture generates a greater increase in electrical conductivity, for temperatures below 11,000 K. The dynamic viscosity of the plasma decreases as the percentage of $AgSnO_2$ alloy electrical contact vapour increases in the mixture, for temperatures below 12,000 K. In the temperature range from 500 K to 20,000 K, the total thermal conductivity of the plasma decreases as the percentage of $AgSnO_2$ alloy electrical contact vapour increases in the mixture. For temperatures between 20,000 K and 30,000 K, the various plasmas of air- $AgSnO_2$ mixtures have almost identical thermal conductivities.

An effective extinguishing medium is defined as one that concurrently exhibits, with respect to its transport coefficients, at least the following properties: high thermal conductivity and low electrical conductivity that diminishes with increasing temperature. By comparing the characteristics of a good extinguishing medium to those of the air plasma contaminated by electrical contact vapours in $AgSnO_2$ alloy studied, we can note that the increase in the percentage of electrical contact vapour in $AgSnO_2$ alloy will slow down the extinction of the electric arc created inside the circuit breaker, especially beyond 0.1% of vapour. This slowing down of the extinction of the electric arc can cause the circuit breaker to fail to cut the electrical current.

However, a plasma radiation study of air-AgSnO₂ mixtures might be necessary to better appreciate the influence of AgSnO₂ alloy vapours on the extinction of the arc created.

5. REFERENCES

- 1. Abbaoui, M. et al. (1985). Influence of the nature of the metal on the conductivity of an argon-metal plasma. *J. Phys. D: Appl. Phys.*, 18, 159–165. https://doi.org/10.1088/0022-3727/18/10/002
- Cheminat, B. & Andanson, P. (1985). Conduction in an electric arc column contaminated by copper vapour. J. Phys D: Appl. Phys., 18, 2183–2192, https://doi.org/10.1088/0022-3727/18/11/008
- 3. Andanson, P. & Lefort, A. (1984). Calculations of electrode erosion by vaporisation of the cathode spot. *J. Phys. D: Appl. Phys.*, 17, 2377–2386. https://doi.org/10.1088/0022-3727/17/12/006

- 4. Lago, F. (2004). *Modelisation to the interaction of an electric arc with a surface : Application to a lightning stroke of an aircraft.* PhD diss., Université Paul Sabatier, France.
- 5. Aubreton, A. (2002). *Modelling and experimental study of a metallic plasma created by laser ablation*. PhD diss., Université Paul Sabatier, Toulouse III, France.
- 6. Bonhomme, A. (2005). Comportement à l'usure de pastilles de contacts électriques à matrice argent. PhD diss., Ecole Nationale Supérieure des Mines, Paris.
- Vicinisvarri, I. et al. (2017). Study of structural properties and defects of Ni-doped SnO₂ nanorods as ethanol gas sensors. *Nanotechnol.*, 28, 265702. https://doi. org/10.1088/1361-6528/aa731c
- 8. Sokovykh, E. V. et al. (2017). Influence of conditions of Pd/SnO₂ nanomaterial formation on properties of hydrogen sensors. *Nanoscale Res. Lett.*,12, 383. https://doi.org/10.1186/s11671-017-2152-3
- 9. Vicinisvarri, I. et al. (2019). A comparative study of structural and ethanol gas sensing properties of pure, nickel and palladium doped SnO₂ nanorods synthesised by the hydrothermal method. *J. Phys. Sci.*, 30(1), 127–143. https://doi.org/10.21315/jps2019.30.1.10
- 10. Yee Kin, C. E. (2015). Study of electrical arcs and their impact on electrical contact materials for power DC applications. PhD diss., Université de Rennes 1, Rennes.
- 11. Pinard, D. J. et al. (1994). Physical and chemical properties of metal oxide additions to AgSnO₂ contact materials and predictions of electrical performance. *IEEE Transactions on Components and Packaging Technol. Part A*, 17(1), 17–23. https://doi.org/10.1109/95.296363
- 12. Abbaoui, M. et al. (2018). Modèle enthalpique de Stephan pour l'étude du pied d'arc cathodique. *J. Int. de Technol., de l'innovation de la physique, de l'énergie et de l'environnement*, 4, 1–16. https://doi.org/10.18145/jitipee.v4i1.138
- 13. Jingqin, W. et al. (2022). Properties of AgSnO₂ contact materials doped with different concentrations of Cr. *Mater.*, 15(14), 4793. https://doi.org/10.3390/ma15144793
- 14. Koalaga, Z. (1991). Contribution to experimental and theoretical study of laminar electric arc plasmas. PhD diss., Université Blaise Pascal, Clermont-Ferrand.
- 15. Kagoné, A. K. (2012). Caractérisation théorique de plasmas thermiques d'arc électrique de mélanges d'air et de vapeur d'eau : Application au disjoncteur basse et moyenne tension. PhD Diss., Université Joseph KI-ZERBO, Ouagadougou, Burkina Faso.
- Banouga, A. et al. (2022). Equilibrium composition of a plasma in the low voltage air circuit breaker contaminated by the vapor of AgSnO₂ alloy electrical contacts. *Adv. Mater. Phys. Chem.*, 12(5), 69–81, https://doi.org/10.4236/ampc.2022.125006
- 17. Colombo, V. et al. (2008). Thermodynamic and transport properties in non-equilibrium argon, oxygen and nitrogen thermal plasmas. *Prog. Nucl. Energy*, 50(8), 921–933. https://doi.org/10.1016/j.pnucene.2008.06.002
- 18. Colombo, V. et al. (2009). Two-temperature thermodynamic and transport properties of argon–hydrogen and nitrogen–hydrogen plasmas. *J. Phys. D: Appl. Phys.*, 42, 055213. https://doi.org/10.1088/0022-3727/42/5/055213
- 19. Colombo, V. et al. (2011). Two-temperature thermodynamic and transport properties of carbon-oxygen plasmas. *Plasma Sources Sci. Technol.*, 20, 035003. https://doi.org/10.1088/0963-0252/20/3/035003

- 20. Devoto, R. S. (1966). Transport properties of ionized monatomic gases. *Phys. Fluids*, 9(6), 1230–1240. https://doi.org/10.1063/1.1761825
- 21. Cressault, Y. (2001). *Thermal plasmas properties in Argon-Hydrogen-Copper mixtures*. PhD diss., Université Toulouse III Paul Sabatier.
- Capitelli, M. et al. (2012). Fundamental aspects of plasma chemical physics transport. Springer New York: Heidelberg Dordrecht London. https://doi.org/10.1007/978-1-4419-8182-0
- 23. Devoto, R. S. (1967). Simplified expressions for the transport properties of ionized monatomic gases. *Phys. Fluids*, 10(10), 2105. https://doi.org/10.1063/1.1762005
- 24. Capitelli, M. (1977). Transport properties of partially ionized gases. *J. Phys. Colloques*, 38, C3-227–C3-237. https://doi.org/10.1051/jphyscol:1977325
- Muckenfuss, C. & Curtiss, C. F. (1958). Thermal conductivity of multicomponent gas mixtures. J. Chem. Phys., 29, 1273–1277. https://doi.org/10.1063/1.1744709
- 26. Ouajji, H. et al. (1986). Composition and conductivity of a copper-air plasma. *J. Phys. D: Appl. Phys.*, 19, 1903–1916. https://doi.org/10.1088/0022-3727/19/10/015
- Kagoné, A. K. et al. (2012). Calculation of air-water vapor mixtures thermal plasmas transport coefficients. *Mater. Sci. Eng.*, 29, 012004. https://doi.org/10.1088/1757-899X/29/1/012004
- 28. Kagoné, A. K. et al. (2020). Transport coefficients of Air-PMMA mixtures thermal plasmas. *American J. Mater. Sci. Eng.*, 8(1), 22–28. https://doi.org/10.12691/ajmse-8-1-4
- 29. Pafadnam, I. et al. (2023). Calculation of fluoroalkylamines transport coefficients used in agriculture and medicine in the context of plasma incineration. *Int. J. Phys.*, 11(5), 253–260, https://doi.org/10.12691/ijp-11-5-4
- 30. Kohio, N. et al (2014). Calculation of transport coefficients of air-water vapor mixtures thermal plasmas used in circuit breakers. Int. *J. Eng. Res.*, 3(12), 711–715.
- 31. André, P. et al. (2004). Transport coefficients of plasmas consisting of insulator vapours Application to PE, POM, PMMA PA66 and PC. *Eur. Phys. J. Appl. Phys.*, 169–182. https://doi.org/10.1051/epjap:2004007
- 32. Aubreton, J. & Fauchais, P. (1983). Influences des potentiels d'interaction sur les propriétés de transport des plasmas thermiques : Exemple d'application le plasma argon hydrogène à la pression atmosphérique. *Rev. Phys. Appl.*, 18(1), 51–66. https://doi.org/10.1051/rphysap:0198300180105100
- 33. Yun, K. S. et al. (1962). High-temperature transport properties of dissociating nitrogen and dissociating oxygen. *Phys. Fluids*, 5(6), 672–678. https://doi.org/10.1063/1.1706683
- 34. Hertz, W. (1971). Experimental determination and interpretation of the conductance decay of interrupted cylindrical arcs. *J. Phy. A Hadrons Nucl.*, 245, 105–125. https://doi.org/10.1007/BF01402333
- 35. Kohio, N. (2016). Etude des propriétés thermodynamiques et des coefficients de transport des plasmas de mélanges d'air et de vapeur d'eau dans la gamme de température 500 K à 12000 K: Applications aux disjoncteurs basse et moyenne tensions. PhD diss., Université Joseph KI-ZERBO, Burkina Faso.

- 36. Yaguibou, W. C. et al. (2019). Coefficients de transport des plasmas air dans un disjoncteur électrique. *J. Phys. de la soaphys*, 1, 1–5. https://doi.org/10.46411/jpsoaphys.19.01.011
- 37. Tan, C. W. (1963). Thermodynamic and transport properties of non-equilibrium partially ionized monoatomic gases. PhD diss., University of Illinois.
- 38. Kihara, T. et al. (1960). Transport properties for gases assuming inverse power intermolecular potentials. *Phys. Fluids*, 3(5), 715–720. https://doi.org/10.1063/1.1706115
- 39. André, P. et al. (2007). Transport coefficients of Ag-SiO₂ plasmas. *Plasma Chem. Plasma Process.*, 27, 381–403. https://doi.org/10.1007/s11090-007-9086-y
- 40. Neufeld, P. D. et al. (1972). Empirical equations to calculate 16 of the transport collision integrals Ω^* (l,s) for the Lennard-Jones (12–6) potential. *J. Chem. Phys.*, 57(3), 1100–1102. https://doi.org/10.1063/1.1678363
- 41. Poling, B. E. et al. (2004). The properties of gases and liquids. McGraw-Hill: USA.
- 42. Yaguibou, W. C. et al. (2018). Impact of aerosol on transport coefficients of air thermal plasmas in circuit breakers. *Int. J. Eng. Res.*, 7(4), 43–47. https://doi.org/10.5958/2319-6890.2018.00094.6
- 43. Hirschfelder, J. O. et al. (1954). *Molecular theory of gases liquids*. John Wiley and Sons Inc., New-York.
- 44. Liboff, R. L. (1959). Transport coefficients determined using the shielded Coulomb potential. *Phys. Fluids*, 2(1), 40–46. https://doi.org/10.1063/1.1724389
- 45. Banouga, A. et al. (2024). Détermination des propriétés thermodynamiques d'un plasma d'air contaminé par de la vapeur d'alliage AgSnO₂. *Canadian J. Phys.*, 102(4), 1–10. https://doi.org/10.1139/cjp-2023-0052
- 46. Capitelli, M. et al. (2000). Transport properties of high temperature air in local thermodynamic equilibrium. *Eur. Phys. J.*, 11, 279–289. https://doi.org/10.1007/s100530070094
- 47. Boulos, M. I. et al. (1994). *Thermal plasmas fundamentals and applications*. Springer International Publishing: Switzerland. https://doi.org/10.1007/978-1-4899-1337-1